

A STOCHASTIC ALGORITHM FOR HIGH SPEED CAPACITANCE EXTRACTION IN INTEGRATED CIRCUITS

Y. L. LE COZ and R. B. IVERSON

Department of Electrical, Computer and Systems Engineering, Rensselaer Polytechnic Institute, Troy, NY 12180-3590, U.S.A.

(Received 21 November 1990; in revised form 27 February 1991; received for publication 29 August 1991)

Abstract—We present the theory of a novel stochastic algorithm for high-speed capacitance extraction in complex integrated circuits. The algorithm is most closely related to a statistical procedure for solving Laplace's equation known as the floating random-walk method. Overall computational efficiency stems from various factors: suitability to rectilinear geometries, statistical-error cancellation, selective integration over Gaussian surfaces and direct capacitance-matrix evaluation. Our analysis begins with Laplace's equation for a scalable square domain, subject to arbitrary Dirichlet conditions. A boundary-integral solution is then found, from which are obtained integrals for electric potential and electric field at the domain center. An electrode-capacitance integral is next derived. This integral is expanded as an infinite sum, and probability rules that statistically evaluate the sum are deduced. These rules define the algorithm. Three sources of numerical error associated with the algorithm have been identified. They are series-truncation error, space-discretization error and statistical error. All these errors can be adequately controlled through proper adjustment of algorithm parameters.

1. INTRODUCTION

Future technological improvements in circuit integration will make electrical connections just as important as the devices they join. It is commonly accepted that electrical performance of integrated circuits will be limited, not by device-switching speed, but by signal propagation along connection paths. Circuit designers will therefore require software "tools" that can rapidly extract capacitance, inductance and resistance in the complex 2- and 3-D geometries typical of integrated circuits. With these thoughts in mind, we propose a highly efficient stochastic algorithm for extracting capacitance in structures with numerous randomly-oriented electrodes.

Before discussing capacitance extraction in further detail, we will first decompose the integrated-circuit electrical connections into a set of idealized mathematical objects. For the most part the set comprises electrodes, corresponding to electrical connections themselves, and dielectrics, corresponding to various insulating layers. We must now solve Laplace's equation[1] for this system. Usually, Laplace's equation is solved for a series of electrode potentials, after which electric fields and interelectrode capacitances are found. Numerical solution of Laplace's equation is generally required, since integrated-circuit geometries are complex and, to a certain extent, arbitrary. Conventional solution methods are deter-

ministic, employing most often finite-difference, finite-element, spectral or boundary-integral discretizations[2-5]. In 2- and 3-D[†] these methods are computationally practical as long as the geometry is relatively simple, possessing few electrodes and dielectrics. However, for complex integrated-circuit geometries these methods are computationally prohibitive.

To resolve this difficulty, we propose a random-walk algorithm that directly evaluates the interelectrode capacitance matrix. The algorithm most closely resembles the floating random-walk method[6,7] for solving the Laplace equation. It is particularly efficient in complex rectilinear geometries, in 2- and, even more so, in 3-D. It has the added advantage of statistically estimating the electric field only in regions where it is needed—the Gaussian surfaces surrounding each electrode. The fact that statistical errors in the electric field tend to cancel during Gaussian-surface integration enhances algorithm efficiency as well. Importantly, when evaluating the capacitance matrix, our algorithm requires a number of Gaussian-surface integrations equal to the total electrode number. Usual capacitance-extraction procedures, in contrast, require on order of the square of such as many integrations. We note lastly that, owing to its stochastic nature, the algorithm readily parallelizes for speed improvement.

Hereafter, we will assume a 2-D rectilinear geometry and neglect variation in electric permittivity. That these assumptions are essential is in no way true; they

[†]The 1-D case is of no interest here.

are made solely for technical simplicity and ease of exposition.[†]

The sections that follow constitute the theory of our algorithm for capacitance extraction. We begin with Laplace's equation over a scalable square domain, subject to arbitrary Dirichlet conditions. A boundary-integral solution is then found, from which are obtained integrals for electric potential and electric field at the domain center. An electrode-capacitance integral is next derived. This integral is expanded as an infinite sum, and probability rules that statistically evaluate the sum are deduced. These rules define the algorithm. Finally, we close our discussion with a few comments concerning numerical errors and their control.

2. LAPLACE'S EQUATION ON A SQUARE

Consider the 2-D Laplace equation

$$\nabla^2 \psi = \frac{\partial^2 \psi}{\partial x^2} + \frac{\partial^2 \psi}{\partial y^2} = 0, \quad (1)$$

for $\psi = \psi(x, y)$, subject to Dirichlet conditions along the square boundary of Fig. 1. We use x and y to denote points inside the square. Points on the boundary S are denoted $[x(\eta), y(\eta)]$, where η is a parameter. We define η to measure boundary length starting from $(0, 0)$ and running counterclockwise; clearly, for a square of size a , $0 \leq \eta \leq 4a$.

Substituting $\psi = X(x) Y(y)$ into (1) yields the ordinary differential equations $(d^2X/dx^2) + k^2 X = 0$ and $(d^2Y/dy^2) - k^2 Y = 0$, where k^2 is the constant of separation[1]. Suppose we prescribe the Dirichlet conditions $\psi[x(\eta), y(\eta)] = \psi_s(\eta)$, an arbitrary function, for $0 < \eta < a$; and $\psi[x(\eta), y(\eta)] = 0$ for $a \leq \eta \leq 4a$. Solutions satisfying both the separated ordinary differential equations and the homogeneous boundary condition have the form $X(x) = \sin(kx)$ and $Y(y) = \sinh[k(a-y)]$, and only then if k takes on the values $n\pi/a$, where n are the positive integers. Using linearity and superposition, we construct all possible solutions to (1) satisfying our homogeneous condition as

$$\psi(x, y) = \sum_{n=1}^{\infty} A_n \sin\left(\frac{n\pi x}{a}\right) \sinh\left[\left(\frac{n\pi}{a}\right)(a-y)\right]. \quad (2)$$

The constants A_n have yet to be specified.

We are left with matching the above solution to the remaining inhomogeneous boundary condition over

[†]Extension to 3-D along with possible inclusion of abrupt changes in electric permittivity result only in minor changes to the algorithm presented here. Nonrectilinear geometries can always be described with piecewise rectilinear constructions. A large class of present-day integrated circuits possess rectilinear geometries, a property that greatly improves our algorithm's performance (as will be seen).

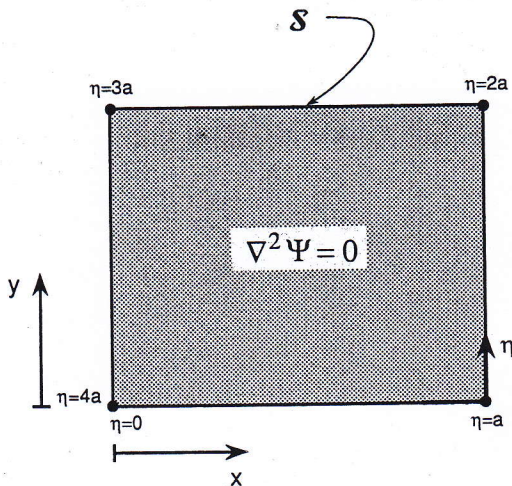


Fig. 1. A square domain for Laplace's equation; η parameterizes the boundary S .

$0 \leq \eta \leq a$. Evaluating sum (2) at $[x(\eta), y(\eta)] = (\eta, 0)$ implies

$$\psi_s(\eta) = \sum_{n=1}^{\infty} A_n \sin\left(\frac{n\pi\eta}{a}\right) \sinh(n\pi). \quad (3)$$

The boundary function ψ_s is assumed piecewise continuous, so that Fourier sum (3) converges. Multiplying both sides of (3) by $\sin(m\pi\eta/a)$; setting $m = 1, 2, \dots$; and integrating from $\eta = 0$ to $\eta = a$; fixes the A_n . These A_n can then be substituted back into (2), which, after interchanging the order of integration and summation, yields

$$\psi(x, y) = \int_0^a d\eta g(x, y|\eta) \psi_s(\eta). \quad (4)$$

We call g the surface Green's function[1] for the boundary parameterized by $0 \leq \eta \leq a$. It has the mathematical form

$$g(x, y|\eta) = \frac{2}{a} \sum_{n=1}^{\infty} \frac{\sinh[(n\pi/a)(a-y)]}{\sinh(n\pi)} \times \sin\left(\frac{n\pi x}{a}\right) \sin\left(\frac{n\pi\eta}{a}\right). \quad (5)$$

Actually, we desire an integral expression valid for arbitrary inhomogeneous conditions over the entire boundary S . By rotating our coordinate system about an axis centered at $x = y = a/2$ through multiple angles of $\pi/4$, we can construct solutions for the other three boundary sides. Their derivation is virtually identical to that just given for the first boundary side. Linearity and superposition permits us to write ψ as an integral over all S :

$$\psi(x, y) = \int_S d\eta G(x, y|\eta) \psi_s(\eta). \quad (6)$$

The complete Green's function G is a sum of four infinite series—the first given by (5), and the other three by similar expressions.

The following facts will prove useful in the next section's discussion. If we arbitrarily translate S_a , the potential at its new center can be defined in terms of the Green's function $\bar{G}(a|\eta)$. This function enables us to express center potential $\bar{\psi}$ as an integral of boundary potential

$$\bar{\psi} = \int_{S_a} d\eta \bar{G}(a|\eta) \psi_{S_a}(\eta). \quad (7)$$

Equation (7) holds for *any* (nonrotated) square-domain S_a of edge-size a , independent of the center position. There also exists a relation between G and \bar{G} , that is

$$\bar{G}(a|\eta) = G(\frac{1}{2}a, \frac{1}{2}a|\eta). \quad (8)$$

Note, the function \bar{G} is normalized to unity over S_a :

$$\int_{S_a} d\eta \bar{G}(a|\eta) = 1. \quad (9)$$

Equation (9) is true, independent of a . This follows by setting $\psi_{S_a}(\eta) = 1$ in (7), for which $\psi(x, y) = \bar{\psi} = 1$.

We will need, as well, expressions similar to (7) for x and y components of the electric field. To obtain them, we differentiate $\psi(x, y)$ in (6)

$$\begin{aligned} E_x(x, y) &= -\frac{\partial}{\partial x} \psi(x, y) \\ &= -\int_S d\eta \frac{\partial}{\partial x} G(x, y|\eta) \psi_S(\eta), \\ E_y(x, y) &= -\frac{\partial}{\partial y} \psi(x, y) \\ &= -\int_S d\eta \frac{\partial}{\partial y} G(x, y|\eta) \psi_S(\eta). \end{aligned} \quad (10)$$

In practice, the Green's function derivatives are evaluated analytically by differentiating, term by term, the sum of four infinite series composing G . Translating S_a as before generates the Green's functions $\bar{G}_x(a|\eta)$ and $\bar{G}_y(a|\eta)$. These integration kernels give electric-field components at the center of a square domain S_a

$$\begin{aligned} E_x &= \int_{S_a} d\eta \bar{G}_x(a|\eta) \psi_{S_a}(\eta), \\ E_y &= \int_{S_a} d\eta \bar{G}_y(a|\eta) \psi_{S_a}(\eta). \end{aligned} \quad (11)$$

Like (7), equations (11) are valid for fields at the center of any (nonrotated) square domain of edge

[†]Diagonal elements C_{11}, C_{22}, \dots represent what we call electrode "self-capacitances". They serve no use in electrical modeling.

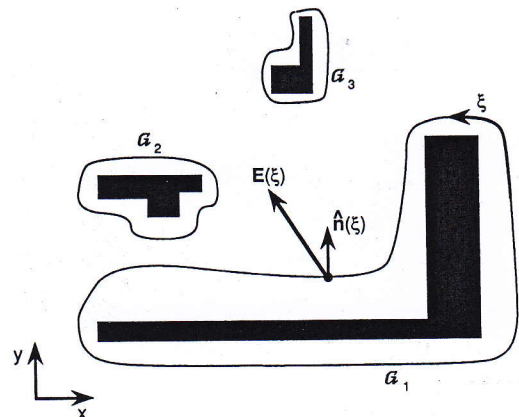


Fig. 2. An example of a 2-D rectilinear electrode arrangement. Gaussian boundaries are denoted G_1 , G_2 and G_3 . The parameter ξ measures length along any of the boundaries. Note also electric field E and outward unit normal \hat{n} both depend on ξ .

size a , independent of center position. Relations exist among G , \bar{G}_x and \bar{G}_y as well. They are

$$\begin{aligned} \bar{G}_x(a|\eta) &= -\frac{\partial}{\partial x} G(\frac{1}{2}a, \frac{1}{2}a|\eta), \\ \bar{G}_y(a|\eta) &= -\frac{\partial}{\partial y} G(\frac{1}{2}a, \frac{1}{2}a|\eta). \end{aligned} \quad (12)$$

3. CAPACITANCE MATRIX

We will now deduce an expression for the electrode-capacitance matrix. Figure 2 is an example electrode arrangement. These 2-D electrodes are shown in black, their edges parallel to the xy -coordinate axes. It is understood that the electrodes extend infinitely in the $+z$ and $-z$ directions. For N electrodes, off-diagonal elements of the capacitance-matrix C_{ij} , $i \neq j, \dagger$ are defined according to

$$q_i = \sum_{j=1}^N C_{ij} (v_i - v_j), \quad (13)$$

where $i = 1, \dots, N$. Above, the v_1, \dots, v_N and q_1, \dots, q_N denote electrode voltages and their corresponding charges *per unit length* in z . Appropriately, C_{ij} is a capacitance *per unit length* in z as well.

Gauss's law permits us to write

$$q_i = \epsilon \int_{G_i} d\xi E(\xi) \cdot \hat{n}(\xi), \quad (14)$$

where ϵ is a constant electric permittivity and G_i is a Gaussian boundary (actually a Gaussian-surface cross section) surrounding a single electrode i . The parameter ξ measures boundary length on which electric field E and outward unit normal \hat{n} depend. Figure 2 shows this parameterization.

We can rewrite (14) by replacing each component of E with its integral equivalent. We will express these components as an integral along the edges of a square $S_{a(\xi)}$ parallel to the coordinate axes and

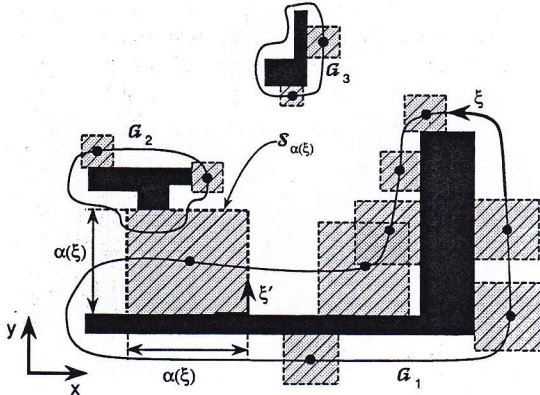


Fig. 3. Examples of initial maximal squares. Boundaries $S_{\alpha(\xi)}$ are of edge size $\alpha(\xi)$ and are centered on Gaussian-boundary points (•).

centered about any particular boundary point on G_i . For each ξ , the square will be chosen as the largest possible containing no electrodes. The square's boundaries thus conform, at least in part, to the electrode boundaries themselves. Figure 3 give examples of such constructions.

Denoting the edge size of these maximal squares as $\alpha(\xi)$, we can use (11) to expand (14) as a double integral. To this end,

$$q_i = - \int_{G_i} d\xi s_i(\xi) \int_{S_{\alpha(\xi)}} d\xi' w(\xi|\xi') \times \bar{G}[\alpha(\xi)|\xi'] \psi_{S_{\alpha(\xi)}}(\xi'). \quad (15)$$

At each electrode $i = 1, \dots, N$ we have defined a weight function

$$w(\xi|\xi') = -\epsilon \frac{\hat{n}_x(\xi)\bar{G}_x[\alpha(\xi)|\xi'] + \hat{n}_y(\xi)\bar{G}_y[\alpha(\xi)|\xi']}{s_i(\xi)\bar{G}[\alpha(\xi)|\xi']} \quad (16)$$

Above, \hat{n}_x and \hat{n}_y are components of \hat{n} . For reasons that will become clear later, we have also introduced the sampling-functions $s_i(\xi)$, which do not affect the value of charge-integrals (15). These functions are assumed normalized over the G_i

$$\int_{G_i} d\xi s_i(\xi) = 1, \quad (17)$$

but are yet unspecified.

To deduce our capacitance algorithm, we must express the q_i in terms of electrode potentials. We begin by splitting the domain $S_{\alpha(\xi)}$ into two parts, examples of which are shown in Fig. 4. The first $S_{\alpha(\xi)}$ is the electrode part, and the second $\tilde{S}_{\alpha(\xi)}$ is the nonelectrode part. Equation (15) can then be written

[†]To simplify notation, we suppress the dependence of $\alpha(\xi')$ on ξ . In general, we have $\alpha(\xi^{\dots\dots\dots}) = \alpha(\xi, \xi', \dots, \xi^{\dots\dots\dots})$.

[‡]Higher-order additive terms in (18) are generated with a simple recursive sequence: (i) copy the last known term; (ii) place a *tilde* over its rightmost integral limit; and (iii) replace $\psi_{S_{\alpha(\xi^{\dots\dots\dots})}}(\xi^{\dots\dots\dots})$ within it by $\int_{S_{\alpha(\xi^{\dots\dots\dots})}} d\xi^{\dots\dots\dots} \bar{G}[\alpha(\xi^{\dots\dots\dots})|\xi^{\dots\dots\dots}] \psi_{S_{\alpha(\xi^{\dots\dots\dots})}}(\xi^{\dots\dots\dots})$.

as a sum of two integrals, one over $S_{\alpha(\xi)}$ and the other over $\tilde{S}_{\alpha(\xi)}$. The nonelectrode potential $\psi_{S_{\alpha(\xi)}, (\xi')}$ in the latter integral can be replaced. We do so with the aid of (7). Note carefully, we must cast (7) with a new dummy variable ξ'' , and we choose $\tilde{S}_{\alpha(\xi)}$ as the new integration domain. Also, we have extended our domain-construction procedure as shown in Fig. 4. Geometrically, $S_{\alpha(\xi)}$ is the largest square, containing no electrodes, centered about any particular boundary point on $\tilde{S}_{\alpha(\xi)}$. If this entire process—splitting $S_{\alpha(\xi)}$ into $S_{\alpha(\xi)}$ and $\tilde{S}_{\alpha(\xi)}$, expanding as a sum of two integrals and replacing the non-electrode-boundary potential by means of (7)—is repeated indefinitely, one obtains an infinite sum of nested integrals:[‡]

$$\begin{aligned} q_i = & - \int_{G_i} d\xi s_i(\xi) \\ & \times \left\{ \int_{S_{\alpha(\xi)}} d\xi' w(\xi|\xi') \bar{G}[\alpha(\xi)|\xi'] \psi_{S_{\alpha(\xi)}}(\xi') \right. \\ & + \int_{\tilde{S}_{\alpha(\xi)}} d\xi' w(\xi|\xi') \bar{G}[\alpha(\xi)|\xi'] \\ & \times \int_{S_{\alpha(\xi')}} d\xi'' \bar{G}[\alpha(\xi')|\xi''] \psi_{S_{\alpha(\xi')}}(\xi'') \\ & + \int_{\tilde{S}_{\alpha(\xi')}} d\xi'' w(\xi|\xi') \bar{G}[\alpha(\xi)|\xi'] \\ & \times \int_{S_{\alpha(\xi'')}} d\xi''' \bar{G}[\alpha(\xi')|\xi'''] \psi_{S_{\alpha(\xi'')}}(\xi''') + \dots \right\}. \quad (18) \end{aligned}$$

Expansion (18) depends only on electrode potentials. Grounding all electrodes except the j th, which we set to some arbitrary voltage v_j , reduces (13) to

$$C_{ij} = -\frac{q_i}{v_j}, \quad (19)$$

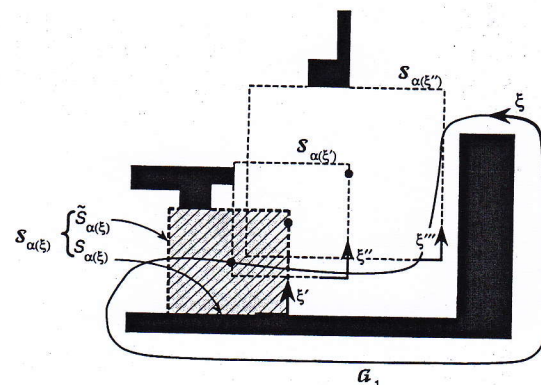


Fig. 4. Examples of subsequent maximal squares (initial square shaded). Each boundary $S_{\alpha(\xi^{\dots\dots\dots})}$ can be decomposed into an electrode part $S_{\alpha(\xi^{\dots\dots\dots})}$ and a non-electrode part $\tilde{S}_{\alpha(\xi^{\dots\dots\dots})}$. These squares are centered on previous square-boundary points (•).

for $i = 1, \dots, N$ ($i \neq j$). Since the q_i of (18) are linear functions of v_j , C_{ij} can be written as an integral expansion independent of v_j . This argument is valid for any possible j ; thus, off-diagonal elements of the capacitance matrix are independent of electrode voltages, and we have

$$\begin{aligned} C_{ij} = & \int_{G_i} d\xi s_i(\xi) \left\{ \int_{S_{\alpha(\xi)}^j} d\xi' w(\xi|\xi') \bar{G}[\alpha(\xi)|\xi'] \right. \\ & + \int_{S_{\alpha(\xi)}} d\xi' w(\xi|\xi') \bar{G}[\alpha(\xi)|\xi'] \\ & \times \int_{S_{\alpha(\xi')}} d\xi'' \bar{G}[\alpha(\xi')|\xi''] \\ & + \int_{S_{\alpha(\xi)}} d\xi'' w(\xi|\xi') \bar{G}[\alpha(\xi)|\xi''] \\ & \times \int_{S_{\alpha(\xi')}} d\xi'' \bar{G}[\alpha(\xi')|\xi''] \\ & \left. \times \int_{S_{\alpha(\xi')}} d\xi''' \bar{G}[\alpha(\xi')|\xi'''] + \dots \right\}. \quad (20) \end{aligned}$$

The boundary† $S_{\alpha(\xi)}^{j\dots\dots}$ is simply the portion of $S_{\alpha(\xi)}^{j\dots\dots}$ coincident with electrode j .

4. EXTRACTION ALGORITHM

In practice, direct evaluation of (20) is computationally prohibitive, especially for integrated-circuit geometries where N is usually large. We resolve this difficulty with a stochastic algorithm that estimates the C_{ij} :

1. Partition each integration variable in (20) into small segments of possibly different size $\Delta\xi_r^{j\dots\dots}$ ($r = 1, 2, \dots$). Define corresponding discrete variables at each segment center $\xi_r^{j\dots\dots}$.
2. Set $\mathcal{N}_i = \mathcal{W}_{ij} = 0$ for all ij ($i, j = 1, \dots, N$). Set $i = 1$.
3. Randomly pick a ξ_r , say ξ_* , on G_i , with discrete probability distribution $P_\xi(\xi_r) = \int_{\Delta\xi_r} d\xi s_i(\xi)$.
4. Randomly pick a ξ'_r , say ξ'_* , on $S_{\alpha(\xi_*)}^j$, with discrete probability distribution, conditioned by ξ_* , $P_{\xi'}(\xi_*|\xi'_r) = \int_{\Delta\xi'_r} d\xi' \bar{G}[\alpha(\xi_*)|\xi']$.

†We mean the superscript “ $\dots\dots$ ” to possibly include the unprimed case. That is, $\xi^{j\dots\dots}$ is one of ξ, ξ', ξ'', \dots

‡This applies to all occurrences of ξ , regardless of subscripts and superscripts. For example, $P_\xi(\xi_*|\xi') = \int_{\Delta\xi_r} d\xi' \bar{G}[\alpha(\xi_*|\xi')] \rightarrow P_{\xi'}(\xi'_*|\xi') = \int_{\Delta\xi'_r} d\xi'' \bar{G}[\alpha(\xi'_*|\xi'')]$. Once Step 4 has been properly changed it remains so until otherwise stated. Note also, $S_{\alpha(\xi^{j\dots\dots})} = S_{\alpha(\xi_r, \xi'_r, \dots, \xi''_r)}$ in Step 4, where $\xi_*, \xi'_*, \dots, \xi''_*$ are the set of random picks before entering or re-entering Step 4.

§Higher-order walks can be constructed in analogous fashion. Notice, for nontrivial electrode geometries the enumeration can range to infinite order.

5. If the last variable picked in Step 4 is not on an electrode boundary, then change Step 4 as follows: mark every occurrence of ξ with an additional prime “ $'$ ” and repeat Step 4.‡
6. If the last variable picked in Step 4 is on the j th electrode boundary, then replace \mathcal{N}_i with $\mathcal{N}_i + 1$ and \mathcal{W}_{ij} with $\mathcal{W}_{ij} + w(\xi_*|\xi'_*)$.
7. If \mathcal{N}_i is sufficiently large, go to Step 8. Else, change Step 4 to its original form (written here above) and go to Step 3.
8. $C_{ij} = \mathcal{W}_{ij}/\mathcal{N}_i$ for $j = 1, \dots, N$. If $i = N$, then stop. Else, replace i with $i + 1$, change Step 4 to its original form (written here above), and go to Step 3.

We will now explain why this capacitance-extraction algorithm works. For a given starting electrode i , enumerate a possible set of \mathcal{N}_i random trajectories, or “walks”, generated by the algorithm that start on G_i and end on any electrode. Figure 5 gives examples of such first-order ($\xi_* \rightarrow \xi'_*$), second-order ($\xi_* \rightarrow \xi'_* \rightarrow \xi''_*$), and third-order ($\xi_* \rightarrow \xi'_* \xi_* \rightarrow \xi''_* \rightarrow \xi'''_*$) walks.§

Consider, for the moment, a subset of this enumeration consisting of first-order walks ending on a specific electrode j . Of the \mathcal{N}_i total walks starting from G_i , $\mathcal{N}_i \times P_\xi(\xi_r)$ of them start at ξ_r . Of those, a fraction $P_{\xi'}(\xi'_r|\xi_r)$ end at ξ'_r on $S_{\alpha(\xi_r)}^j$. Therefore, the total number of walks from ξ_r to ξ'_r is simply $\mathcal{N}_i \times P_\xi(\xi_r) \times P_{\xi'}(\xi'_r|\xi_r)$. The algorithm sums $w(\xi_r|\xi'_r)$ over all possible ξ_r, ξ'_r -pairs and divides by \mathcal{N}_i , giving

$$C_{ij}^{(1)} \approx \frac{\mathcal{W}_{ij}^{(1)}}{\mathcal{N}_i} = \sum_{\xi_r} P_\xi(\xi_r) \sum_{S_{\alpha(\xi_r)}^j} w(\xi_r|\xi'_r) P_{\xi'}(\xi'_r|\xi_r). \quad (21)$$

The sums in (21) are to be taken over discrete points ξ_r and ξ'_r on their respective surfaces G_i and $S_{\alpha(\xi_r)}^j$. In addition, we have designated first-order-walk contributions with the superscript “(1)”. Observe that (21) and the discussion preceding it are valid for any starting Gaussian surface and ending electrode, that is, any ij -pair ($i \neq j$). Remember, as well, that (21) is a good approximation to $C_{ij}^{(1)}$ when \mathcal{N}_i is large—large

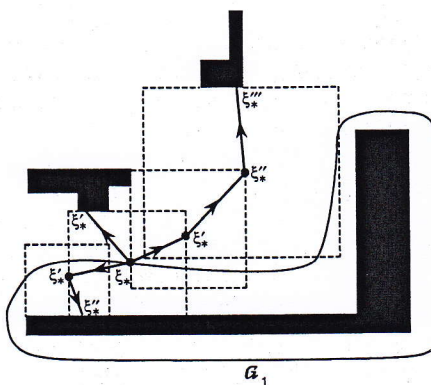


Fig. 5. Examples of first-, second- and third-order walks. For clarity, the walks have been drawn to start at the same G_i -boundary-point ξ_* .

enough to ensure that the known probability distributions P_ξ and $P_{\xi'}$ adequately represent the *actual* distributions in our enumeration of walks.

A connection with (20) follows upon replacing P_ξ and $P_{\xi'}$ in (21) with their integral equivalents from Steps 3 and 4 of the algorithm. We get

$$C_{ij}^{(1)} \approx \sum_{G_i} \left[\int_{\Delta\xi_r} d\xi s_i(\xi) \right] \times \sum_{S_{\alpha(\xi_r)}^j} w(\xi_r | \xi') \left\{ \int_{\Delta\xi'} d\xi' \bar{G}[\alpha(\xi_r) | \xi'] \right\}. \quad (22)$$

The $\Delta\xi'$ are assumed small enough so that $w(\xi_r | \xi')$ varies little over their extent. This permits us to change ξ' to ξ in w and to move w within the rightmost integrand of (22). Hence

$$C_{ij}^{(1)} \approx \sum_{G_i} \left[\int_{\Delta\xi_r} d\xi s_i(\xi) \right] \sum_{S_{\alpha(\xi_r)}^j} \int_{\Delta\xi'} d\xi' w(\xi_r | \xi') \bar{G}[\alpha(\xi_r) | \xi']. \quad (23)$$

Now, evaluating the right-most sum above, we find immediately

$$C_{ij}^{(1)} \approx \sum_{G_i} \left[\int_{\Delta\xi_r} d\xi s_i(\xi) \right] \times \int_{S_{\alpha(\xi_r)}^j} d\xi' w(\xi_r | \xi') \bar{G}[\alpha(\xi_r) | \xi']. \quad (24)$$

Lastly, if we assume the $\Delta\xi$ are small enough, so that the rightmost integral in (24) varies little over their extent, we can change ξ , to ξ in w , \bar{G} and α ; and move the integral within the leftmost integrand. Evaluating the remaining sum, as before, gives our final result:

$$C_{ij}^{(1)} \approx \int_{G_i} d\xi s_i(\xi) \int_{S_{\alpha(\xi)}^j} d\xi w(\xi | \xi') \bar{G}[\alpha(\xi) | \xi']. \quad (25)$$

The expression above is a first-order approximation to C_{ij} , in other words, the first term in expansion (20). The general proof for the n th term, $C_{ij}^{(n)}$, in (20) proceeds along lines similar to (21)–(25) and is left to the reader.[†]

The algorithm actually sums w for walks of varying order n . Consequently, it generates a statistical estimate of C_{ij} by summing statistical estimates of $C_{ij}^{(n)}$ over n . Mathematically, we have

$$C_{ij} \approx \sum_{n=1}^{\infty} C_{ij}^{(n)} = \frac{1}{N_i} \sum_{n=1}^{\infty} \mathcal{W}_{ij}^{(n)} = \frac{\mathcal{W}_{ij}}{N_i}, \quad (26)$$

[†]It would begin, for any specific n , with a subset of our initial enumeration consisting solely of n th-order random walks.

[‡]For N_i sufficiently large, the sums in (26) will span a wide range of orders, n . In actual numerical implementations, low-sample-number or even missing estimates for some $C_{ij}^{(n)}$ will generally occur (N_i is finite, but n has an infinity of values). Nevertheless, the resulting error is negligible as long as N_i remains large.

where $\mathcal{W}_{ij}^{(n)}$ is the sum of weight-functions w for all n th-order random walks starting on Gaussian boundary G_i and ending on electrode j .[‡]

We turn now to a brief discussion concerning the numerical errors associated with the extraction algorithm. In principle, each source of error is controllable and can be made sufficiently small. We survey the three important types of numerical error associated with the algorithm—series truncation, space discretization and statistical.

Algorithm probability distributions derive from an infinite-series Green's function; only a finite number of terms can be kept in a numerical implementation. This results in series-truncation error. It is controlled by keeping a greater number of terms in any finite-series approximation.

Space-discretization error stems from the finite size of integration-variable segments $\Delta\xi$. This type of error is controlled by making the $\Delta\xi$ small, particularly in regions where fields and potentials vary rapidly.

The last source of numerical error is statistical error. The algorithm's stochastic nature causes this error—specifically, the finite value of N_i . When N_i is large, statistical error will be minimized. Additional control of statistical error can be achieved by means of the sampling functions s_i introduced in (15) and (16). Step 3 of the algorithm uses these functions as probability distributions for sampling Gaussian boundaries. Choosing a set of s_i , whose values become relatively large where electric fields vary rapidly, will further minimize statistical error.

5. CONCLUSION

We have presented a novel stochastic algorithm for high-speed capacitance extraction in integrated circuits. Details of its mathematical formulation and a brief discussion of its associated numerical errors have been given in Sections 2–4. We close with a list highlighting the algorithm's key features:

- **Efficient in complex rectilinear geometries**—The algorithm performs random walks on square boundaries that conform, exactly, to rectilinear electrode boundaries. Only a few random “steps” are required to terminate a typical walk, even in complicated arrangements.
- **Statistical-error cancellation**—Errors due to statistical fluctuations tend to cancel during electric-field determination. Additional cancellation occurs during the final integration process for capacitance.
- **Selective Gaussian-surface integration**—Electric flux is estimated at electrode Gaussian surfaces, and nowhere else within the domain. Gaussian-surface integrals are evaluated in a selective and thus highly efficient manner.

- *Direct capacitance-matrix evaluation*—Usual inversion of a linear set of equations is avoided. The capacitance matrix is computed directly with a minimum number of Gaussian-surface integrations (equal to the total electrode number).
- *Simplicity and extendability*—The algorithm is relatively easy to code on a computer. It also extends, in a simple and efficient way, to three dimensions, including domains with piecewise-continuous dielectrics.†
- *Parallelizable*—Random walks are statistically independent; the algorithm is a prime candidate for speed optimization using parallel-processing techniques.

Acknowledgement—The authors are indebted to Professor J. D. Meindl, not only for sponsoring this work, but also for his helpful technical discussions and consistent encouragement.

REFERENCES

1. P. M. Morse and H. Feshbach, *Methods of Theoretical Physics (Part I)*. McGraw-Hill, New York (1953).
2. A. H. Zemanian, *IEEE Trans. Electron Devices* **35**, 985 (1988).

†These remarks are based on preliminary calculations we have performed, in both 2- and 3-D.

3. P. E. Cottrell and E. M. Buturla, *IBM J. Res. Dev.* **29**, 277 (1985).
4. F. S. Lai, *Solid-St. Electron.* **32**, 141 (1989).
5. A. E. Ruehli and P. A. Brennan, *IEEE Trans. Microwave Theory Tech.* **MTT-21**, 76 (1973).
6. G. M. Brown, *Modern Mathematics for Engineers* (Edited by E. F. Beckenbach). McGraw-Hill, New York (1956).
7. A. Haji-Sheikh and E. M. Sparrow, *Trans. ASME C-89*, 121 (1967). (See, in particular, the section "Authors Closure", and references therein).

APPENDIX

Preliminary Results

We present here some of our initial numerical results.

The example we give is based on a simple extension of the theory from 2- to 3-D. Proper numerical implementation and computer coding was verified by comparison with available analytical solutions for a parallel-plate geometry. The algorithm accuracy was found to be less than 2% (discretization error plus truncation error).

Figure A1 illustrates the type of 3-D electrode geometry that was used. Wires 1 and 2 cross at right angles; both run parallel to a ground plane. Mathematically, the structure is treated as periodic in the horizontal plane, with the unit cell of Fig. A1. For convenience, we set $\epsilon = 1 \text{ pF}/\mu\text{m}$. Wire cross-sections are $1 \times 4 \mu\text{m}$. Wire lengths and ground-plane edge sizes for a unit cell are all $40 \mu\text{m}$. (Periodic extension is therefore on $40 \mu\text{m}$ centers.) The separation distance between wire 1 and wire 2 and between wire 2 and the ground plane is $1 \mu\text{m}$.

We report in Table A1 two coupling capacitances for wire 2 in a unit cell: C_{21} , that with respect to wire 1, and C_{2g} , that with respect to the ground plane. Results are also cited for two additional cases, in which either wire 1 or the ground

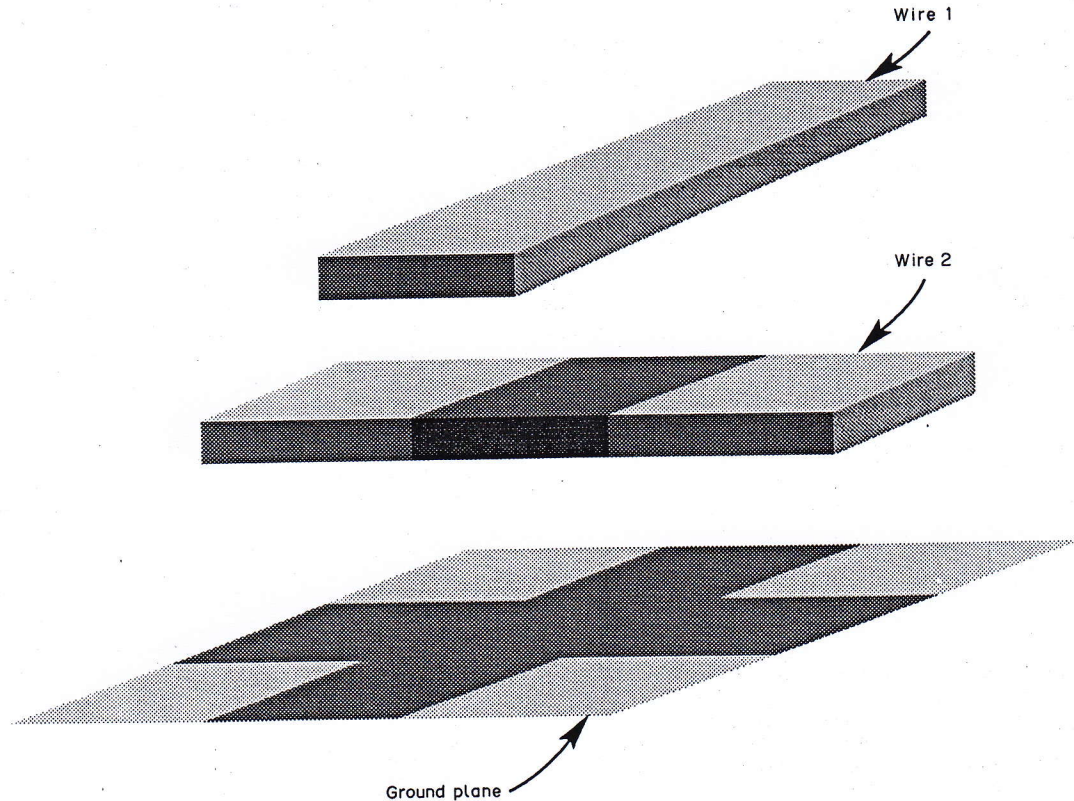


Fig. A1. A 3-D cross-wire geometry and associated ground plane.

plane is removed. A fixed number of 9400 walks was performed for each of the three cases. The associated statistical errors were roughly 5%. CPU time for each case was nearly 40 s on a MAC IIIfx personal computer. The computer executes at a rate of 0.3 MFLOPS (Mat-Lab benchmark).

Table A1. Calculated coupling capacitances

	Wire 1 + Wire 2 + Ground Plane	Wire 1 + Wire 2	Wire 2 + Ground Plane
C_{21}	$50 \pm 3 \text{ pF}$	$105 \pm 10 \text{ pF}$	—
C_{2g}	$265 \pm 8 \text{ pF}$	—	$305 \pm 15 \text{ pF}$